Indian Journal of Chemistry
Vol. 61, February 2022, pp. 121-126

Comparison study of preferential oxidation of CO over nanocrystalline Cu/CeO_2 catalysts synthesized by different preparation methods

Shubhadeep Adak[a,b], Md Sarfaraz Ahmad[a], Souvik Sadhu[a], Rubina Khatun[a,b], V V D N Prasad[a,b] & Rajaram Bal[a,b,*]

[a]Light Stock Processing Division, CSIR-Indian Institute of Petroleum, Dehradun 248 005, India

[b]Academy of Scientific and Innovative Research, Ghaziabad, Uttar Pradesh- 201 002, India

*E-mail: raja@iip.res.in

Received 12 July 2021; revised and accepted 27 January 2022

Preferential oxidation of carbon monoxide in presence of excess hydrogen is a promising alternative to restrict the CO deposition in the Pt-anode in the practical polymer electrolyte membrane fuel cell application. In the present work, nanocrystalline copper-ceria catalysts have been synthesized by hydrothermal method, wet impregnation method and urea nitrate combustion method. Their characterizations have been carried out by using X-ray diffraction, transmission electron microscopy, X . ray photoelectron spectroscopy-It has been found that Cu^{2+} replaced Ce^{4+} in cerium oxide, creating oxygen vacancy. The formation of more nano-sized CeO_2 leads to more oxygen vacancies in CeO_2 through the formation of interfacial Cu^{1+} ions, which also enhances the CO oxidation activity. Among the synthesized Cu-CeO_2 catalysts, the catalyst prepared by hydrothermal method have shown both CO conversion andC O_2 selectivity as 100% towards CO oxidation at 373 K in the presence of excess H_2 making this catalyst viable for practical fuel cell application..

Keywords: Cu-CeO_2, PROX, CuO, CeO_2, Nanoparticles, Oxygen vacancy

The possible consequences of climate change are grave and, more importantly, irreversible. As a result, a renewable energy-dependent zero-emission future should be the top focus[1,2]. Because hydrogen is carbon-free with high energy density and low environmental impact, it is seen as viable alternative energy and is commonly exploited to generate power[3]. In this respect, the H_2-feed fuel cell has gained a lot of attention as a clean energy source for generating electricity without emitting greenhouse gases[4]. Hydrogen, on the other hand, is regarded as a secondary energy source generated from the transformation of other energy sources. Methane is a suitable as well as an acceptable fuel to generate H_2 due to its high H/C proportion and available natural gas pipeline network. Furthermore, hydrogen transmission and storage issues have prompted the development of reformers in miniature scale for on-site and on-demand H_2 synthesis[5]. As a result, distributed H_2 generation by reformer systems in miniature scale is critical for fuel cell automobiles[6]. CO must be eliminated from the reforming gas to less than 100 ppmv in polymer electrolyte membrane fuel cells (PEMFCs) because carbon monoxide is a toxin to anode[7]. The preferential oxidation (PROX) reaction is used in the fuel generator of fuel cells to obtain CO clean hydrogen to alleviate this problem[8]. For polymer electrolyte membrane fuel cell (PEMFC) application, the catalyst should work below 403 K as the decomposition temperature of the membrane is ~ 403 K. Although there are several reports in the literature using different catalysts, in most of the cases, either catalyst shows low activity or low O_2 selectivity or deactivates very fast. In this work, we have synthesized nanocrystalline Cu/CeO_2 catalysts by different preparation methods and found that catalyst prepared by hydrothermal method showed 100% CO conversion and 100% H_2 selectivity in presence of excess H_2, making this catalyst viable for practical fuel cell application.

Experimental Details

Catalyst preparation

Impregnation method for Cu-CeO_2 preparation

Cu loading on ceria was carried out using the following method. 0.2661 g copper nitrate trihydrate was made soluble in 10 mL distilled water. Then 0.0375 g cetyltrimethylammonium bromide (CTAB) was made soluble in 1 mL distilled water and 1 ml ethanol. After that, the addition of the CTAB solution to the copper nitrate solution was done, followed by adding the Cu containing solution to 2 g commercial

cerium oxide dispersed in 20 mL distilled water (by 10 minutes sonication) and stirred for 2 h. Then the mixture was dried at 353 K overnight. Finally, the produced solid was crushed, and calcination was performed at 823 K for 5 h in air. The catalyst is denoted as 3.5% Cu-CeO_2^{IMP}.

Hydrothermal method for Cu-CeO_2preparation

In this experiment, 0.2661 g $Cu(NO_3)_2.3H_2O$ and 4.8691 g $Ce(NO_3)_3.6H_2O$ were stirred and made soluble in distilled water of 100 mL to form a clear pale blue coloured solution. NaOH solution (5N) was added dropwise to adjust pH≈9 in the resulting mixture. Then H_2O-EtOH solution (50% ethanol) of CTAB was added under vigorous stirring (1500 rpm) for one hour to form a bluish-green gel. Finally, 0.03 g polyvinylpyrrolidone (PVP) solution in 1 mL aqueous ethanol (50%) was added to the gel under stirring for 2 h. The weight ratio in the final gel was Cu:CTAB:PVP:H_2O=0.07:0.1:0.03:100. The resulting mixture was treated hydrothermally in an autoclave vessel (stainless-steel) having Teflon lining at 448 K for 24 h. Then, the autoclave was brought down to the ambient atmosphere, and the solid material was filtered and water-washed until pH of filtrate becomes 7 and dried for 8 h at 393 K. The final solid material was crushed, and calcination was performed in air at 823 K for 6 h to get Cu-CeO_2 catalyst. The catalyst is denoted as 3.5%Cu-CeO_2^{HYD}.

Combustion method for Cu-CeO_2 preparation

For the synthesis of 2 g of 3.5% Cu-CeO_2, at first, 0.2661 g of $Cu(NO_3)_2.3H_2O$ and 4.8691 g $Ce(NO_3)_3.6H_2O$ were dissolved into 20 mL of distilled water. After 15 min mixing of solution, urea (molar ratio of urea and nitrate was 2.50) was added to the solution, followed by heating the mixed solution to 353 K for 10 min. A viscous gel was obtained when placed in a muffle furnace at 673 K, combustion started and released smoke. After combustion, a powder obtained which was further heated at 773 K for 2 h. The catalyst is denoted as 3.5%Cu-CeO_2^{COMB}.

Catalyst characterization

Different techniques of characterization like XRD, SEM, TEM and XPS were used to characterize the catalyst thoroughly. A PROTO X-ray diffractometer fitted with a Lynx eye high-speed strip detector and a Cu Kα radiation source was used to record the powder X-ray diffraction pattern. Diffraction patterns at a rate of 0.5 degrees (2θ) per minute in the 2°-80° region were recorded. A JEOL JEM 2100 microscope was used to collect the TEM images, and dispersion of the sample in ethanol mounted on a lacey carbon formvar-coated Cu grid was used to prepare the samples. Energy-dispersive X-ray spectroscopy (EDX) along with TEM was used to carry out the elemental analysis.A Thermo Scientific K-Alpha X-ray photoelectron spectrometer was used to record the X-ray photoelectron spectroscopy (XPS), and binding energies (±0.1 eV) were established with respect to the position of C 1s peak at 284.6 eV.

Catalytic activity

Activities of the fresh nano-composites as catalysts for PROX reaction were examined in a fixed-bed flow reactor with a GHSV = 4000-20,000 h^{-1}. The flow of gas constituting of O_2:CO:He:H_2=1:2:47:50 (in mol%) was used as the reactant. Before the CO-PROX reaction, pre-treatment of the tested sample was in reductive (20%H_2/He) conditions at 573 K for 60 min was followed by the commencement of activity test experiments as described below. The effluent gas compositions were determined with an on-line gas chromatograph (TRACE-GC 700 series, Thermo Fischer Scientific) coupled with a TCD. A column channel did separation of the tested gases in the GC. A column of Unibeads C coupled to that channel separated CO, O_2, CO_2 and water vapour. Considering that the total volumes of the reaction gas before and after PROX remained almost unchanged (< 1 vol. %), the CO conversions were calculated according to the following equations:

$$\text{CO conversion (\%)} = \frac{nCO_{in} - nCO_{out}}{nCO_{in}} \times 100\% \quad ...(1)$$

CO_2 selectivity equation is given as

$$CO_2 \text{ selectivity (\%)} = \frac{nCO_{in} - nCO_{out}}{O_{2in} - O_{2out}} \times 100\% \quad ...(2)$$

where CO_{in}, O_{2in} and CO_{out}, O_{2out} are the GC response peak areas of CO and O_2 before and after the reaction. In the experiment, we used a quartz tube of 5.8 mm diameter and length 10 cm as the reactor. Gas flow is controlled by a thermal mass flow controller (TMFC), and water vapour was controlled by a water bubbler (in which temperature is maintained by a thermostat). The whole tubing is heated with the help of a thermostat and heating tape to vaporize all the gases and liquid water.

Results and Discussion

Catalyst Characterization

The X-ray diffraction patterns of Cu-CeO_2 catalysts along with commercial CeO_2 (JCPDS 81-0792) are shown in Fig. 1. The XRD peaks corresponding to the 2θ values of 28.5º, 33.1º, 47.6º, 56.4º correspond to characteristic CeO_2 formation. The peaks of CuO (JCPDS 89-5899) appear at 2θ values of 35.5º and 38.7º, corresponding to (111) which are not present in the catalysts due to low Cu-loading (3.5wt% Cu). The XRD of the spent catalyst (post 100 h of time-on-stream) 3.5%Cu-CeO_2^{HYD} catalyst shows characteristic peaks of CeO_2 at 28.5º, 47.6º, 56.4º without changing its phase, which confirms the thermal stability of the support material.

SEM elemental mapping confirmed the presence of copper (Fig. 2b). The homogeneous distribution of Cu is confirmed by elemental mapping (Fig. 2c). TEM images of 3.5%Cu-CeO_2^{IMP} and 3.5%Cu-CeO_2^{COMB} are given in Fig. S1 and Fig. S2, respectively, in the Supplementary Data. From TEM images, we can see the particle size distribution is 5 nm to 15 nm (Fig. S3-(5) and (6)). From SAED we can say that the 3.5% Cu-CeO_2^{HYD} is polycrystalline in nature, where we can see the particle are agglomerated and bigger in size as compared to the 3.5% Cu-CeO_2^{HYD}.

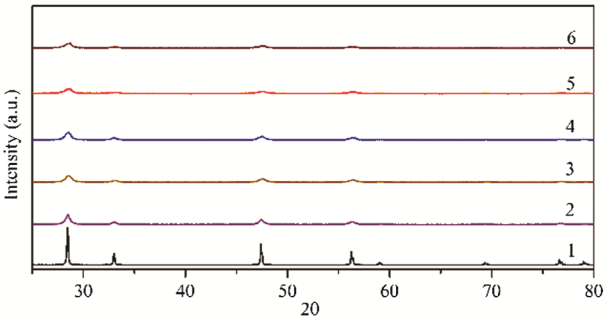

Fig. 1 — XRD patterns of ceria and Cu-supported ceria catalysts. [1, commercial CeO_2; 2, prepared CeO_2; 3, 3.5%Cu-CeO_2^{IMP}; 4, 3.5%Cu-CeO_2^{COMB}; 5, 3.5%Cu-CeO_2^{HYD}; 6, spent catalyst 3.5%Cu-CeO_2^{HYD} after 100 h]

To explore the nature of surface of the prepared catalysts, XPS analysis of 3.5%Cu-CeO_2^{HYD} nanoparticles was also carried out (Fig. 3). XPS analysis confirms the Ce 3d core level peak, as shown in Fig. 4, which is entirely consistent with the previously reported work[9]. It has been observed that Ce^{3+} is formed due to the creation of oxygen vacancies. Nanoparticles have an enhanced effect on oxygen vacancies because a greater fraction of particles on the surface has small size, and the surface atoms' coordination has been decreased[10]. Greater number of O_vacancies in the 3.5%Cu-CeO_2^{HYD}catalyst is illustrated by the XPS results. A higher ratio of O_vacancies and hydroxyl (-OH) groups to $O_{lattice}$ indicates the enhancement of the content of vacant surface oxygen and a hydroxyl group via the presence of requisite amounts of Cu. However, further increment of the copper contents would lower the surface O_2 vacancy contents because of copper oxide (CuO) formation on the CeO_2surface. Origin and PeakFit software were employed for the fitting of XPS spectra of 3.5%Cu-CeO_2^{HYD} catalyst to

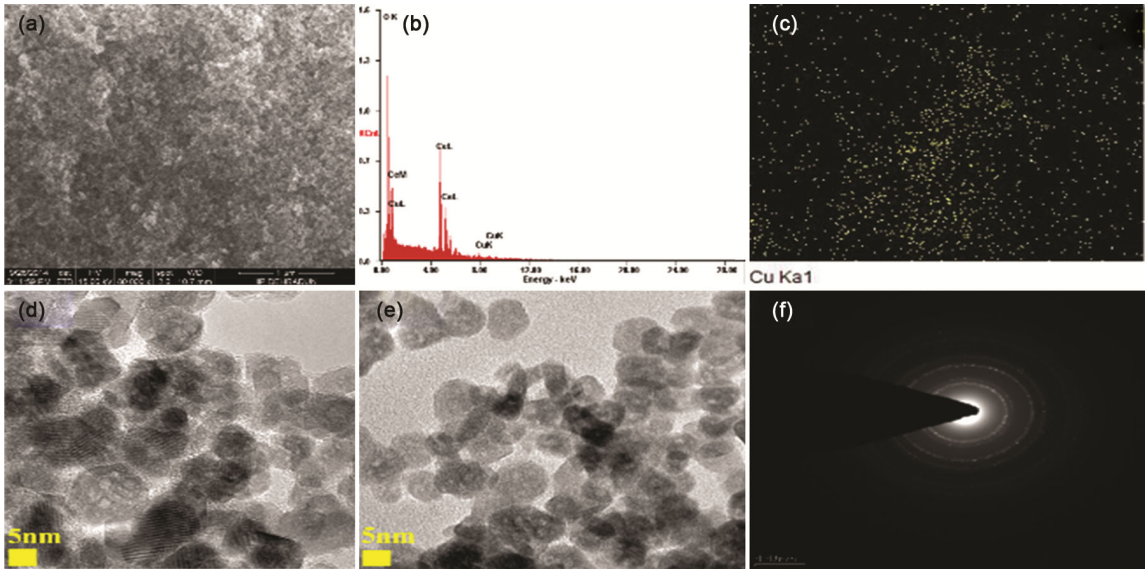

Fig. 2 — SEM of (1) 3.5%Cu-CeO_2^{HYD}; (2) Elemental mapping of 3.5%Cu-CeO_2^{HT} from SEM; (3) Elemental mapping of Cu in 3.5%Cu-CeO_2^{HYD} from SEM; (4) TEM image of fresh catalyst 3.5%Cu-CeO_2^{HYD} (5) TEM image of spent catalyst 3.5%Cu-CeO_2^{HYD} after 100 h; (6) SAED pattern of 3.5%Cu-CeO_2^{HYD} catalyst

Gaussian-Lorentzian functions to determine the peak positions, line widths & relative areas of the Cu, Ce and O species quantitatively (Fig. 3, 4 and 5). Cu XPS spectra for fresh 3.5%Cu-CeO_2^{HYD}catalyst (Fig. 3), a considerable amount of interfacial Cu^{1+}species with a binding energy value of 930.5 eV is present (Fig. 3a), and the intensity of this peak increases for the spent

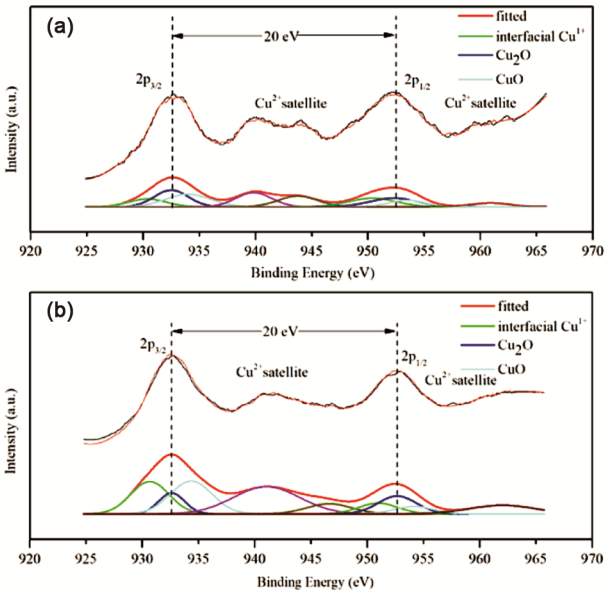

Fig. 3 — XPS spectra of 3.5%Cu-CeO_2^{HYD}, deconvoluted copper species of (a) fresh sample and (b) spent sample after 100 h reaction

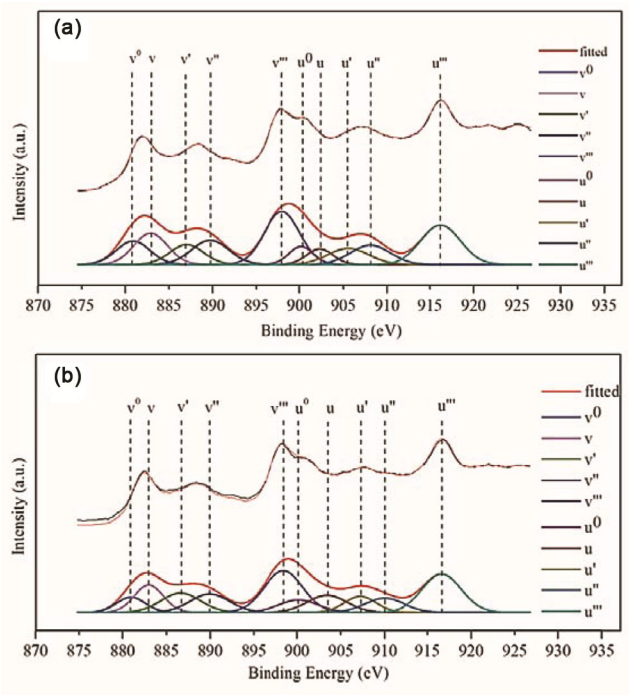

Fig. 4 — XPS spectra of 3.5%Cu-CeO_2^{HYD}, deconvoluted cerium species of (a) fresh sample and (b) spent sample after 100 h reaction

catalyst, indicating the formation of more interfacial Cu species during catalysis[11]. Cu_2O (932.1 eV), CuO (933.2 eV) are also present. Cu^{2+} and Cu^{1+} species are responsible for CO oxidation and form an equilibrium Cu^{2+}fi Cu^{1+} (recreation of Cu^{1+} sites and replenishment of oxygen vacancies by molecular oxygen involved in successive catalytic cycles) if there is no deactivation.The Ce XPS spectra comprise six peaks which correspond to the three spin-orbit doublet pairs, CeO_2 consists of both valences ($3^+$and 4^+) due to being highly non-stoichiometric.

Binding energies of 915.8 eV, 897.2 eV. 889.0 eV and 881.5 eV constitute the primary peaks of Ce^{4+} $3d_{3/2}$ and Ce^{4+} $3d_{5/2}$, correspondingly (Fig. 4a). 906.1 eV for Ce^{3+} $3d_{3/2}$ and 887.4 eV for Ce^{3+} $3d_{5/2}$, correspondingly comprise two new satellite lines, which mean 'shake-up'. Comparing the fresh and spent 3.5%Cu-CeO_2^{HYD}catalyst, it was noticed that the concentration of Ce^{3+} species increased (at positions 905.7 eV, 901.1 eV, 882.9 eV) and decreased (886.2 eV) after the reaction, whereas in the case of Ce^{4+} species concentration decreased at the positions 898.3 eV, 895.2 eV, 880.2 eV) and increased at 889 eV.

This observation concludes that Ce^{4+} to Ce^{3+} reversible transformation, a vital issue in the redox ability of CO is facilitated by the oxygen vacancies. A higher ratio of Ce^{4+}/Ce^{3+} is obvious to be exhibited by Cu-CeO_2 nanoparticles. Earlier reports showed that the ceria surface exhibited variable oxidation states. This may enhance the reduction ability of catalysts to facilitate the electron exchange process rates[12,13].

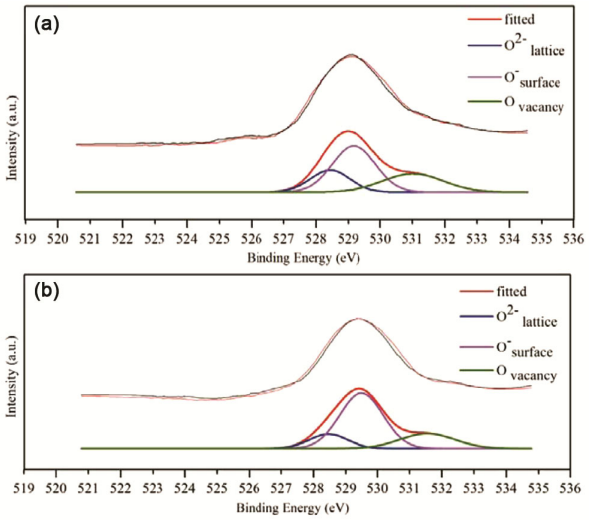

Fig. 5 — XPS spectra 3.5%Cu-CeO_2^{HYD}, deconvoluted oxygen species of (a) fresh sample and (b) spent sample after 100 h reaction

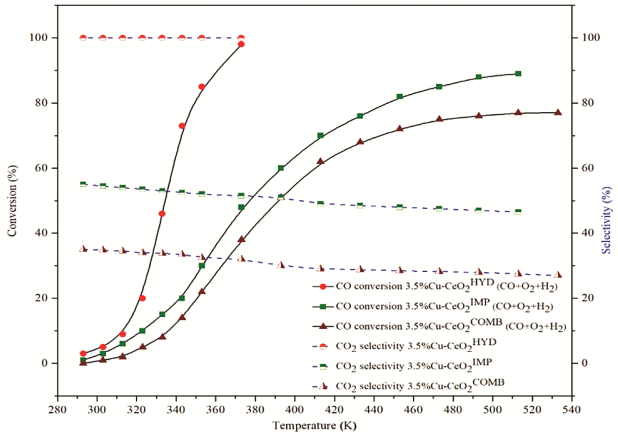

Fig. 6 — CO conversions with $H_2$for 3.5%Cu-CeO_2 catalysts andblue lines stand for CO_2 selectivity for the catalysts in PROX of CO with feed composition O_2:CO:He:H_2=1:2:47:50 at GHSV=20,000 h^{-1}

The integration of copper ions mainly enhanced the contraction of the lattice parameter. Fig.4 shows that Ce 3d spectra curves comprise eight peaks corresponding to four pairs of spin-orbit doublets[14]. The percentage of the addition of areas of the Ce^{3+} ions to the addition of areas of the total cerium species gives us the proportion of Ce^{3+} ions present with respect to the total cerium species[14]. It is known that the oxygen vacancies formation is linked to the presence of Ce^{3+}(Ref. 14,15). Therefore, copper addition increases Ce^{4+} to Ce^{3+} reduction and facilitates oxygen vacancy formation, due to which CuO-CeO_2 catalyst can exhibit enhanced activity for CO selective oxidation.The shift of oxidation states between Ce^{4+} and Ce^{3+} under oxidizing and reducing conditions gives CeO_2 robust oxygen storage and release capacity.

XPS region spectra of O1s on the synthesized Cu-CeO_2 catalyst are displayed in Fig. 5a & b. For fresh sample, 528.4 eV peak corresponds to oxygen ions ($O_{\text{-lattice}}$) in CeO_2. Higher binding energies of 530.5 eV and 531.1 eV gives rise to two shoulders are attributable to oxygen vacancies and hydroxyl groups, respectively (Fig 5a). Similar peak positions are observed in the case of spent catalyst (Fig. 5b). It was noticed that the increase in oxygen vacancies and hydroxyl groups and a decrease of oxygen ions ($O_{\text{-lattice}}$) in CeO_2 (after reaction) happened. We assigned that the hydroxyl groups initiate the reaction through oxygen vacancies, and the deficiency of lattice oxygen species is compensated by feeding oxygen via oxygen vacancy.

Catalytic performance

Catalytic activities of 3.5%Cu-CeO_2^{HYD} and 3.5%Cu-CeO_2^{COMB} and 3.5%Cu-CeO_2^{IMP} are shown in Fig. 6. In presence of excess H_2, the 3.5%Cu-CeO_2^{HYD} catalyst shows 98% CO conversion at 373 K and CO_2 selectivity of 100% in this temperature regime. Whereas 3.5%Cu-CeO_2^{IMP} and 3.5%Cu-CeO_2^{COMB} show CO conversion 89% at 513 K and 77% at 533 K, respectively. CO_2 selectivity of 3.5%Cu-CeO_2^{IMP} is continuously decreasing from 55 to 46% in this temperature regime. In the case of 3.5%Cu-CeO_2^{COMB}, this scenario is 35 to 27% (Fig. 6).

Conclusion

Among the three different nanocrystalline Cu-CeO_2 catalysts, hydrothermally prepared catalyst shows the best catalytic activity with 3.5% Cu-loading. Cu^{2+} has been found to have replaced Ce^{4+} in cerium oxide, resulting in an oxygen vacancy. The formation of additional nano-sized CeO_2 results in more oxygen vacancies in ceria, as well as an increase in CO oxidation activity due to the formation of interfacial Cu^{1+} ions. At 373 K in the presence of excess H_2, the 3.5%Cu-CeO_2^{HYD} catalyst demonstrated 100% CO conversion with 100% CO_2 selectivity towards CO oxidation. The 3.5%Cu-CeO_2^{HYD} catalyst did not deactivate even after 100 h time-on-stream run.

Supplementary Data

Supplementary data associated with this article are available in the electronic form at http://www.nopr.niscair.res.in/jinfo/ijca/IJCA_61(02)YYYY-YYYY_SupplData.pdf.

Acknowledgement

Shubhadeep Adak thanks CSIR-IIP, India, for the fellowship. Md Sarfaraz Ahmad and Souvik Sadhu thank CSIR-IIP, India, for the fellowship. Rubina Khatun thanks CSIR-New Delhi, India, for the fellowship. The Director, CSIR-IIP, is acknowledged for his help and encouragement. The authors thank ASD, CSIR-IIP, for analytical services. Rajaram Bal acknowledges DST, India, for funding the project (DST/TSG/AMT/2015/325).

References

1 European Commission - Karlsruhe (Germany), *Hydrogen energy and fuel cells A vision of our future*, (European Commission, Directorate-General for Energy and Transport, France) 2003, p.10.

2 Veiga S, Romero M, Faccio R, Segobia D, Duarte H, Apesteguía C & Bussi J, *Catal Today*, 344 (2020) 190.

3 Davó-Quiñonero A, Bailón-García E, López-Rodríguez S, Juan-Juan J, Lozano-Castelló D, García-Melchor M, Herrera F C, Pellegrin E, Escudero C & Bueno-López A, *ACS Catal*, 10 (2020) 6532.

4 Park J, Shakkthivel P, Kim H, Han M, Jang J, Kim Y, Kim H & Shul Y, *Int J Hydrog*, 33 (2008) 1845.
5 Lu J, Lei Y, Wan G, Mei Z, Yu J, Zhao Y, He S & Luo Y, *Appl Catal B*, 263 (2020) 118177.
6 Oh S H & Sinkevitch R M, *J Catal*, 142 (1993) 254.
7 Li L, Song L, Wang H, Chen C, She Y, Zhan Y, Lin X & Zheng Q, *Int J Hydrog*, 36 (2011) 8839.
8 Lee Y-L, Jha A, Jang W-J, Shim J-O, Jeon K-W, Na H-S, Kim H-M, Lee D-W, Yoo S-Y, Jeon B-H, Bae J W & Roh H-S, *Top Catal*, 60 (2017) 721.
9 Li H, Wang G, Zhang F, Cai Y, Wang Y & Djerdj I, *RSC Adv*, 2 (2012) 12413.
10 Gamarra D, Belver C, Fernández-García M & Martínez-Arias A, *J Am Chem Soc*, 129 (2007) 12064.
11 Monte M, Munuera G, Costa D, Conesa J C & Martínez-Arias A, *Phys Chem Chem Phys*, 17 (2015) 29995.
12 Li J, Zhu P, Zuo S, Huang Q & Zhou R, *Appl Catal A*, 381 (2010) 261.
13 Wu X, Liang Q, Weng D, Fan J & Ran R, *Catal Today*, 126 (2007) 430.
14 Fan J, Wu X, Wu X, Liang Q, Ran R & Weng D, *Appl Catal B*, 81 (2008) 38.
15 Dutta P, Pal S, Seehra M S, Shi Y, Eyring E M & Ernst R D, *Chem Mater*, 18 (2006) 5144.